Clim. Past Discuss., 7, 1235–1259, 2011
www.clim-past-discuss.net/7/1235/2011/
doi:10.5194/cpd-7-1235-2011

Climate of the Past Discussions

Weakened atmospheric energy transport feedback in cold glacial climates

I. Cvijanovic, P. L. Langen, and E. Kaas

Centre for Ice and Climate, Niels Bohr Institute, University of Copenhagen, Juliane Maries Vej 30, 2100 Copenhagen, Denmark

Received: 10 March 2011 – Accepted: 2 April 2011 – Published: 13 April 2011

Correspondence to: I. Cvijanovic (ivanacv@nbi.ku.dk)

Published by Copernicus Publications on behalf of the European Geosciences Union.

Abstract

The response of atmospheric energy transport during Northern Hemisphere cooling and warming from present day (PD) and Last Glacial Maximum (LGM) conditions is investigated using sea surface temperature anomalies derived from a freshwater hosing experiment. The present day climate shows enhanced sensitivity of the atmospheric energy transport compared to that of the LGM suggesting an ability of the PD atmosphere to reorganize more easily and thereby dampen temperature anomalies that may arise from changes in the oceanic transport. The increased PD sensitivity relative to that of the LGM is due mainly to a stronger dry static energy transport response which, in turn, is driven chiefly by larger changes in the transient eddy heat flux. In comparison, changes in latent heat transport play a minor role in the overall transport sensitivity.

1 Introduction

Proxy climate data from around the world show enhanced variability during glacial periods (e.g. D/O events) compared to the interglacials (e.g., Greenland ice cores (NGRIP Members, 2004), Antarctic ice cores (EPICA Members, 2006), Cariaco Basin sediment cores (Peterson et al., 2000), Asian cave stalagmites (Wang et al., 2001) and Arabian Sea sediment cores (Banakar et al., 2010). Changes in the oceanic circulation and halocline stability (due to, e.g., ice discharge or meltwater events) are considered a potential driver of these abrupt events as inferred from the ocean sediment data and modeling studies (Keigwin et al., 1994; Broecker et al., 1994; Dahl et al., 2005). Although the role of the atmosphere is considered secondary in this regard, various atmospheric and surface feedbacks can enhance or weaken the initial anomaly in the oceanic state. The focus of this study is on a presumably negative feedback, namely the atmospheric heat transport and its response to high northern latitude temperature anomalies under warm interglacial and cold glacial conditions.

CPD
7, 1235–1259, 2011

Numerous modeling studies have addressed communication between high and low latitudes, showing that changes in ice cover, Atlantic Meridional Overturning Circulation (AMOC) or generally antisymmetric interhemispheric heating in the high latitudes can induce a displacement of the ITCZ (Zhang and Delworth, 2005; Chiang and Bitz, 2005; Broccoli et al., 2006; Chiang et al., 2008). In spite of a dominance of atmospheric over oceanic transport in the extratropics (Trenberth and Caron 2001; Wunsch, 2005), possible changes in the sea ice extent due to oceanic transport variations, and their further influence on the atmospheric circulation leave the ocean a relevant trigger for abrupt climate shifts.

The sensitivity of the atmospheric energy transport to global mean temperature and meridional temperature gradients was previously studied by Caballero and Langen (2005) in a series of aquaplanet simulations. They found atmospheric heat transport independent of global mean temperature in cases when the global mean temperature was high and meridional temperature gradient low. These climate states were also the ones in which sensitivity to temperature gradient was largest. Cheng et al. (2007) focused on the atmospheric and oceanic heat transport responses due to AMOC slowdown under LGM and PD conditions. They found the oceanic heat transport largely compensated by the atmospheric heat transport with midlatitude transient eddy transport playing an important role for the overall atmospheric response in both climates. Hwang and Frierson (2010) investigated the atmospheric poleward energy transport under global warming and found the change in atmospheric moisture content and latent heat transport to be the main cause for the total atmospheric transport changes while the dry static energy transport plays a smaller, compensating role.

This study investigates the sensitivity of the atmospheric energy transport to meridional temperature gradients under glacial and interglacial climates. In contrast to the previous studies that compared the transport response in the two climates, we address its actual sensitivity and its ability to feed back negatively on the imposed changes. Variations in temperature gradients were imposed by changes in sea surface temperatures (SST) and sea ice lines (reflecting the sea surface response to oceanic heat

CPD
7, 1235–1259, 2011

transport variations). A weakened atmospheric transport sensitivity, i.e., a less negative atmospheric feedback, would imply a climate state with the atmosphere less capable of damping high latitude temperature anomalies arising from changes in the oceanic transport. In this case, the climate is thus likely to be influenced more strongly by excursions in the oceanic circulation (by spending longer time in cold or warm phases). In an atmospheric general circulation model (AGCM), high latitude SST anomalies are applied mainly in the North Atlantic mimicking the effect of changing AMOC strength. The sensitivity of the atmospheric response to different sea ice extents and SSTs is then tested with the anomalies applied in two background climates (PD and LGM).

2 Experimental configuration

The atmospheric transport sensitivity is tested using the National Center for Atmospheric Research's CCM3 (Kiehl et al., 1998), employing T42 horizontal resolution with 18 levels in the vertical. This AGCM was run in prescribed SST mode with both PD SSTs (Shea et al., 1992) and LGM SSTs (CLIMAP, 1994) in order to obtain the two control simulations. LGM topography and land mask is taken from the ICE-5G reconstruction of Peltier (2004). Experiments have been run for 30 yr and averages over the last 20 yr are used in the analysis. The main parameters describing the experiments are given in Table 1.

SST anomalies are derived from a freshwater hosing experiment in the intermediate complexity model ECBilt-CLIO (Goosse and Fichefet, 1999; Opsteegh et al., 1998). In an experiment similar to that of Renssen et al. (2002), a freshwater forcing of 1.5 Sv was applied to the ECBilt-CLIO for 20 yr in the North Atlantic and SST anomalies are calculated from the difference between the resulting on-state after recovery and the off-state of the AMOC (details are given by Wang, 2009). These annually varying SST anomaly fields are multiplied by a series of different strength factors and added to the two background control fields in the CCM3 (Fig. 1a). A total of 18 experiments were performed: two controls (present day (PD) and Last Glacial Maximum (LGM) and 8 sets

CPD
7, 1235–1259, 2011

of perturbations starting from each. Experiments are named after the strength factor used to multiply the anomaly: prefix *p* refers to positive anomalies (NH warming) and *m* to negative anomalies (NH cooling), with strengths ranging from −2 to 2.

In the simulations, a sea surface temperature of −1.8 °C (freezing point) is used as the criterion to distinguish between the open ocean points and sea ice points of 2 m thickness. Therefore, when preparing the perturbation input fields, surface temperature (T_S) fields from the control experiments were employed at the ocean points to allow for temperatures below −1.8 °C in the presence of sea ice. During summer, however, sea ice T_S may attain values between −1.8 °C and 0 °C, which would imply that a sea ice point is mistaken for an ocean point. To avoid this, we subtracted 1.8 K from the sea ice points with temperatures above the freezing point of sea water. The SST anomaly fields were then added to these control T_S fields and Fig. 1b and c demonstrates the resulting sea ice lines. Note that summer is shown here as it is the season with the highest sea ice decline due to the anomalies imposed.

Although we do impose perturbations that tend to realistically represent the effects of changes in the oceanic heat transport, the important point is not the exact SST and sea ice line geometries which will depend on model and background climate, but the alteration of the large scale Northern Hemisphere meridional temperature gradient (NHTG) obtained in this way. Here we define NHTG as the difference of the average surface temperatures over the areas 0°–30° N and 30°–90° N. Using the NHTG as a metric enables a comparison between the two climates that significantly differ from each other in their surface conditions (different SST fields, sea ice geometries, topography etc.). The SST anomalies applied in the PD and LGM simulations are identical, but the resulting NHTG anomalies are not, because the large LGM sea ice extent with low surface temperatures requires much larger anomalies for open ocean points to emerge. Therefore, the resulting range of the imposed NHTG changes is around 3 K for LGM simulations and 5 K for PD. NHTG values for each experiment are summarized in Table 2. Due to the strength of the coupling between surface and surface air temperature, all conclusions in the following remain unchanged if the surface air tem-

CPD
7, 1235–1259, 2011

perature or lower tropospheric temperature was used instead of surface temperature in the definition of NHTG.

3 Results

3.1 Atmospheric transport sensitivities

Total northward atmospheric and latent energy transports are calculated from the atmospheric energy and fresh water budgets, respectively. Such implied transport calculations assume a steady state with constant (long term) energy and moisture content in the column, which is the case for the multi-year averages used in these calculations. Northward dry static energy transport (DSE) is obtained as the residual between the total atmospheric and latent heat transports. We do not account for the very small kinetic energy transport (it remains a part of the DSE transport). These calculations have been verified by direct calculation using vertical integrals of meridional advection of temperature, water vapor and geopotential (vT, vq and vΦ).

Total transport anomalies at the equator and 30° N are plotted as a function of NHTG anomalies in Fig. 2. Imposed NH warming/cooling (negative/positive NHTG anomalies) causes a decreased/increased total atmospheric transport. Panels a, b and c show total, dry static energy (DSE) and latent cross-equatorial heat transport for PD (solid circles) and LGM (open circles) warming and cooling simulations. Panels d, e and f show the same for the transports across 30° N.

Linear regression coefficients rc (and the corresponding r^2 values) of transport versus NHTG anomalies provide a measure of the sensitivity of the atmospheric transport. Statistical significance of the results was confirmed by Monte Carlo sampling, giving frequency distributions of rc differences between the two climates based on yearly samples. The LGM simulations indicate an enhanced total transport sensitivity at the equator and decreased sensitivity at 30° N relative to PD (Fig. 2a and d). The PD simulations show weaker response at the equator with sensitivity increasing northward and peaking in the mid-latitudes.

CPD
7, 1235–1259, 2011

Separation of the total transport into DSE (Fig. 2b) and latent (Fig. 2c) components reveals the canceling effect that the two have at the equator with DSE giving the sign of the total response in both climates (slopes for DSE are 0.45 PW K^{-1} and 0.68 PW K^{-1} compared to −0.36 PW K^{-1} and −0.47 PW K^{-1} for latent transport, for the PD and LGM cases, respectively). Both components show stronger cross equatorial response in the LGM climate compared to the PD.

At 30° N the PD total response is double that of the LGM with the DSE component being the main cause of the difference (Fig. 2d and e). Compared to the LGM, the PD DSE response is almost three times larger (slopes are 0.16 PW K^{-1} and 0.05 PW K^{-1} for PD and LGM). Latent energy transport (Fig. 2f) shows lower sensitivity compared to DSE (Fig. 2e) in PD simulations. In contrast to this, in LGM simulations DSE and latent transport sensitivities are approximately the same.

An additional experiment, in which three times the initial anomaly was added to the LGM background climate (LM_p3), was performed in order to obtain a NHTG anomaly with a value similar to that in the maximum NH PD warming case (PD_p2). This additional experiment also allows for a comparison between the two climates under similar sea ice extents. This is illustrated in Fig. 2 (in red open circles). The overall slope of the midlatitude LGM response is still much smaller than the PD even when including such an extreme perturbation.

We also tested whether the above findings are valid for the monthly transport anomalies due to the seasonal changes in NHTG (not shown). In comparison with our original experiments with high- to mid-latitude perturbations, the NHTG has much larger variations throughout the course of the year with amplitude close to 30 K. The weakened LGM mid-latitude transport sensitivity to NHTG perturbations remains valid for the monthly values: the response is higher in the PD than in the LGM simulation and this becomes even more pronounced in the higher mid-latitudes. DSE transport remains the main contributor to the total transport sensitivity with enhanced influence over latent transport.

CPD
7, 1235–1259, 2011

3.2 Meridional structure

To further investigate the atmospheric transport response to the imposed perturbations, we consider the meridional structure of the anomalies (Fig. 3). PD total transport anomalies (Fig. 3a) peak around 35° N with larger amplitude than the LGM anomalies (Fig. 3d) whose peak is located close to the equator. Separating the total transport into its two components, we find that the larger anomalies are seen in DSE, both in PD and LGM climates. An interesting feature is the tail in PD DSE transport anomaly (Fig. 3b) that reaches up to 60° N. Here DSE and latent transport anomalies have the same sign and this is thus the main cause of the extratropical peak in the PD net transport anomaly (Fig. 3a). These features are not present in the LGM and the peak in total atmospheric LGM transport (Fig. 3d) comes from a weaker cancellation between equatorial DSE and latent transport changes.

3.2.1 Mid-latitude response

Decomposition of the DSE anomalies into its sensible and potential components (not shown) reveals the canceling effect that the two have, with the sensible heat transport anomaly yielding the sign of the mid-latitude PD DSE response. In contrast, in the LGM simulations both components have much smaller anomalies with the sensible heat transport determining the overall DSE anomaly in lower mid-latitudes and potential energy transport in the higher mid-latitudes. Given that the atmospheric heat transport in mid-latitudes is mainly provided by the eddies, the different responses of the sensible heat transport in the two climates can be explained by considering the stationary and transient eddy heat flux components. Figures 4 and 5 show stationary $\left[\overline{v^*}\,\overline{T^*}\right]$ (upper panels) and transient $\left[\overline{v'T'}\right]$ (lower panels) meridional eddy heat flux anomalies for PD and LGM simulations, respectively (square brackets denote zonal means and overbars time means, primes/stars denote deviations from the time/zonal mean). We find the glacial control climate to have enhanced stationary eddy heat fluxes compared to the

CPD
7, 1235–1259, 2011

PD control and weaker transient eddy heat fluxes (not shown). A similar result was found by Murakami et al. (2008) who saw increased mid-latitude DSE transport during LGM due to increased stationary wave activity. Increased stationary wave activity in LGM has been shown to be caused by the LGM orography (Cook and Held, 1988). Despite the increased stationary eddy heat flux in the glacial control, it is the transient eddy heat flux anomalies that determine the overall eddy heat flux response to the added surface perturbations in both climates (Figs. 4 and 5). With NH cooling/warming, the transient eddy heat flux increases/decreases with the equator to pole temperature gradient, but in the LGM simulations this response is weaker than in PD and displaced towards lower mid-latitudes. Figure 6, showing the vertically integrated transient and stationary eddy heat transport anomalies, confirms this picture of significantly larger transient transport anomalies (left plot) compared to the stationary transport anomalies (right plot) and the enhanced PD response (black lines) compared to the LGM (grey lines).

In conclusion, the cause of the decreased mid-latitude DSE transport sensitivity in cold glacial climates is the decreased sensible heat transport sensitivity, which, in turn, is a consequence of the weakened transient eddy heat flux response. In our LGM simulations we see an enhanced and narrower polar jet (Fig. 7c) and decreased eddy kinetic energy (Fig. 7d) in the North Atlantic compared to the PD simulations (Fig. 7a and b). Other studies (Li and Battisti, 2008; Donohoe and Battisti, 2009) have noted reduced storminess under glacial conditions despite the stronger Atlantic jet which is in line with our findings. The dominance of mid-latitude DSE response in AMOC slow-down experiments was also found by Cheng et al. (2007) who had as well attributed it to increased transient eddy activity. It is important to note the difference to the global warming experiments of Hwang and Frierson (2010), where latent heat flux dominates the overall response.

CPD
7, 1235–1259, 2011

3.2.2 Low-latitude effects

Changes in cross-equatorial energy transports are related to changes in Hadley cell dynamics and shifts in the ITCZ. A more northward/southward ITCZ location results in more energy transported to the Southern/Northern Hemisphere. DSE transport increases towards the cooled hemisphere and latent towards the warmed one. The location of the crossover between the annual latent and DSE transports was found by Trenberth and Stepaniak (2003) to coincide with the time mean location of the ITCZ, and we will exploit that here and use it as a proxy. This is illustrated in Fig. 8 for the PD and LGM simulations as the intersection of lines with the same dash pattern. In PD simulations the crossover is located in the Northern Hemisphere for all of the perturbations. The position is at 5° N in the control, and depending on the perturbation strength it gets displaced northward or southward, while staying in the NH. In contrast, the LGM time mean ITCZ location is closer to the equator and more sensitive to the imposed perturbations such that it shifts all the way to 6° S in the cooling simulation and to 6° N in the warming simulation. The fact that the crossover between the two transports co-locates with the present day ITCZ does not necessarily carry over to LGM conditions, but consideration of the crossovers reveals that there is something essentially different in the energy transport partitioning under glacial and interglacial conditions.

The ability of the Hadley cell to transport energy more or less efficiently can be determined from the total gross moist static stability by using, for example, the ratio between the total energy and mass transports, as done by Kang et al. (2009). In our experiments, the Hadley cells are shifted between the two climates, so we simply use the ratio of the northward energy heat transport at the latitude of the maximum mass stream function and the stream function maximum itself. In this manner we obtain a measure of the northern Hadley cell efficiency in transporting energy to the mid-latitudes, which is directly comparable for PD and LGM conditions. We find that the drier low-level LGM atmosphere increases the total gross moist static stability ($2.6 \times 10^4\,\mathrm{J\,kg^{-1}}$ compared to $2.0 \times 10^4\,\mathrm{J\,kg^{-1}}$ in PD), weakens the canceling effect that the latent heat transport

CPD
7, 1235–1259, 2011

has on the DSE transport and yields a larger LGM total northward transport in the low latitudes compared to the present day. We speculate that this larger efficiency permits the LGM energy transport to respond more readily to the circulation changes imposed by the meridional temperature gradients. Further details behind the different Hadley cell responses in the two climates are beyond the scope of the study.

4 Discussion and conclusion

Our study demonstrates enhanced atmospheric heat transport sensitivity under warm (interglacial) compared to cold (glacial) conditions. This is shown to be a feature of both annual mean transports (in the experiments with added SST perturbations) and of monthly transports (in the control runs, due to seasonal variations of NHTG). The weakened glacial transport sensitivity is linked to a reduced transient eddy heat flux response. In comparison to the PD climate, the glacial climate is found to have stronger overall stationary eddy heat fluxes, weaker transient eddy heat fluxes, a stronger and narrower polar jet and decreased eddy kinetic energy in the North Atlantic. With SST anomalies added in both climates, the transient eddy heat flux responses dominate over those of the stationary eddy heat fluxes, an effect which is larger in PD than in LGM simulations.

Consequently, the PD climate appears more capable of damping high latitude anomalies due to the strong mid-latitude response while much less change is seen in the tropics. In contrast, the LGM simulations display the major response in the tropics where the cancellation between DSE and latent heat transports is weaker and energy is transported more efficiently from the tropics. From Fig. 2 it is possible to estimate the sensitivity of transport convergence into the area 0°–30° N for the PD and LGM experiments. When the NHTG increases by 1 K (as a result of the added surface perturbations), the PD equator sees an increased import of energy from the Southern Hemisphere of 0.09 PW and at 30° N an increased poleward transport of 0.22 PW is seen. The area 0°–30° N thus encounters a net loss of 0.13 PW. In the LGM

CPD
7, 1235–1259, 2011

experiments, the resulting import of energy from the Southern Hemisphere is considerably larger (0.21 PW) and the poleward transport at 30° N is considerably smaller (0.11 PW) and the area 0°–30° N encounters a net *gain* of 0.10 PW. The two effects of the prime LGM response being in the tropics and the prime PD response being in the mid-latitudes thus combine to yield opposite tendencies on the 0°–30° N energy budget with a gain in LGM and a loss in PD. The net contribution to the 30°–90° N budgets from the energy transport are just equal to the 30° N sensitivities, i.e., 0.22 PW for PD and 0.11 PW for LGM. From these quantities we can calculate the energy transport contribution to the tendency on NHTG as the net for the low latitude area less that of the high latitude area. For the PD experiments we find −0.13 PW −0.22 PW = −0.35 PW, and for the LGM we find 0.10 PW – 0.11 PW = −0.01 PW. The contribution of the meridional energy transport to the negative tendency on the NHTG is thus much larger for the PD than for the LGM. In the PD, there is thus a much larger negative feedback on the imposed temperature gradients as a consequence of the enhanced atmospheric transport response.

Although the atmospheric circulation changes are not considered to be the primary cause of decreased interglacial variability, these results give an important indication of a varying ability of the atmosphere to feed back negatively on imposed oceanic changes in different climates. Surface boundary conditions as seen by the atmosphere, i.e., topography, sea ice and SST, are quite different in PD and LGM, and we therefore see a general response that is different during LGM. In order to qualitatively constrain the importance of the sea ice geometry, an additional experiment with three times the initial anomaly added to the LGM background climate was performed. This simulation had much less summer sea ice and a NHTG anomaly similar to that of the PD_p2 case. The overall slope of the LGM response was not affected significantly by the inclusion of this point, but if one considers only the warming LGM simulations (including the LM_p3 experiment), then the slopes in the two climates become more similar. Since these are all cases with less sea ice, the large sea ice extent in LGM simulations is apparently an important component in the decreased glacial energy transport feedback. This is,

CPD
7, 1235–1259, 2011

however, not necessarily the only reason given that according to, for instance, Cook and Held (1988), it is the LGM orography that causes a change in the stationary eddies and thus forces a different partitioning of the transient and stationary components between the two climates.

In conclusion, the sensitivity of the transport to NHTG changes (that depends on the background surface conditions described above) shows less negative transport feedback during LGM as compared to PD. Further work is required to evaluate the described responses when the interactions with the ocean surface are allowed.

Acknowledgements. This work was supported in part by a grant of HPC resources from the Arctic Region Supercomputing Center (ARSC) at the University of Alaska Fairbanks as part of the Department of Defense High Performance Computing Modernization Program. The authors acknowledge the support of the Danish National Research Foundation and thank Peter D. Ditlevsen and John C. H. Chiang for useful discussions as well as Peter Wang for supplying the temperature anomalies associated with the ECBilt-CLIO freshwater experiments.

References

Banakar, V. K., Mahesh, B. S., Burr, G., and Chodankar, A. R.: Climatology of the Eastern Arabian Sea during the last glacial cycle reconstructed from paired measurement of foraminiferal d18O and Mg/Ca, Quat. Res., 73(3), 535–540, doi:10.1016/j.yqres.2010.02.002, 2010.

Broccoli, A. J., Dahl, K. A., and Stouffer, R. J.: Response of the ITCZ to Northern Hemisphere cooling, Geophys. Res. Lett., 33, L01702, doi:10.1029/2005GL024546, 2006.

Broecker, W. S.: Massive iceberg discharges as triggers for global climate change, Nature, 372, 421–424, 1994.

Caballero, R. and Langen, P. L.: The dynamic range of poleward energy transport in an atmospheric general circulation model, Geophys. Res. Lett., 32, L02705, doi:10.1029/2004GL021581, 2005.

Cheng, W., Bitz, C. M., and Chiang, J. C. H.: Adjustment of the global climate to an abrupt slowdown of the Atlantic meridional overturning circulation, in: Ocean Circulation: Mechanisms and Impacts, edited by: Schmittner, A., Chiang, J. C. H., and Hemming, S. R., AGU, Washington, DC, Geophys. Monogr. Ser., 173, 295–313, 2007.

CPD

7, 1235–1259, 2011

Chiang, J. C. H. and Bitz, C. M.: Influence of high latitude ice cover on the marine Intertropical Convergence Zone, Clim. Dynam., 25, 477–496, 2005.
Chiang, J. C. H, Cheng, W., and Bitz, C. M.: Fast teleconnections to the tropical Atlantic sector from Atlantic thermohaline adjustment, Geophys. Res. Lett., 35, L07704, doi:10.1029/2008GL033292, 2008.
CLIMAP: CLIMAP 18K Database, IGBP PAGES/World Data Center for Paleoclimatology Data Contribution Series 94-001, Technical report NOAA/NGDC Paleoclimatology Program, Boulder CO, USA, 1994.
Cook, K. H. and Held, I. M.: Stationary waves of the ice age climate, J. Climate, 1, 807–819, 1988.
Dahl, K. A., Broccoli, A. J., and Stouffer, R. J.: Assessing the role of North Atlantic freshwater forcing in millennial scale climate variability: A tropical Atlantic perspective, Clim. Dynam., 24, 325–346, 2005.
Donohoe, A. and Battisti, D. S.: Causes of reduced North Atlantic storm activity in a CAM3 simulation of the Last Glacial Maximum, J. Climate, 22, 4793–4808, 2009.
EPICA Community Members: One-to-one coupling of glacial climate variability in Greenland and Antarctica, Nature, 444, 195–198, 2006.
Goosse., H., and Fichefet, T.: Importance of ice-ocean interactions for the global ocean circulation: A model study, J. Geophys. Res., 104, 23337–23355, 1999.
Hwang Y. T and Frierson, D. M. W.: Increasing atmospheric poleward energy transport with global warming, Geophys. Res. Lett., 37, L24807, doi:10.1029/2010GL045440, 2010.
Kang, S. M., Frierson, D. M. W., and Held, I. M.: The tropical response to extratropical thermal forcing in an idealized GCM: The importance of radiative feedbacks and convective parameterization, J. Atmos. Sci., 66, 2812–2827, doi:10.1175/2009JAS2924.1, 2009.
Keigwin, L. D., Curry, W. B., Lehman, S. J., and Johnsen, S.: The role of the deep ocean in North Atlantic climate change between 70 and 130 kyr ago, Nature, 371, 323–326, 1994.
Kiehl J. T., Hack, J. J., Bonan, G. B., Boville, B. A., Williamson, D. L., and Rasch, P. J.: The National Center for Atmospheric Research Community Climate Model, CCM3, J. Climate, 11, 1131–1149, 1998.
Li, C. and Battisti, D. S.: Reduced Atlantic Storminess during Last Glacial Maximum: Evidence from a Coupled Climate Model, J. Climate, 21(14), 3561–3579, 2008.
NGRIP members: High-resolution record of Northern Hemisphere climate extending into the last interglacial period, Nature, 432, 147–151, 2004.

CPD
7, 1235–1259, 2011

Murakami, S., Ohgaito, R., Abe-Ouchi, A., Crucifix, M., and Otto-Bliesner, B. L.: Global-Scale Energy and Freshwater Balance in Glacial Climate: A Comparison of Three PMIP2 LGM Simulations, J. Climate, 21(19), 5008–5033, 2008.

Opsteegh J. D., Haarsma, R. J., Selten, F. M., and Kattenberg, A.: ECBILT: a dynamic alternative to mixed boundary conditions in ocean models, Tellus, 50A, 348–367, 1998.

Peltier, W. R.: Global glacial isostasy and the surface of the ice age Earth: The ICE-5G (VM2) model and GRACE, Ann. Rev. Earth Planet. Sci., 32, 111–149, 2004.

Peterson, L. C., Haug, G. H., Hughen, K. A., and Rohl U.: Rapid changes in the hydrologic cycle of the tropical Atlantic during the last glacial, Science, 290, 1947–1951, doi:10.1126/science.290.5498.1947, 2000.

Renssen H., Goose, H., and Fichefet, T.: Modeling the effect of freshwater pulses on the early Holocene climate: The influence of high-frequency climate variability, Paleoceanography, 17(2), 1020, doi:10.1029/2001PA000649, 2002.

Shea, D. J., Trenberth, K. E., and Reynolds, R. W.: A global monthly sea surface temperature climatology, J. Climate, 5, 987–1001, 1992.

Trenberth, K. E. and Caron, J. M.: Estimates of meridional atmosphere and ocean heat transports, J. Climate, 14, 3433–3443, 2001.

Trenberth, K. E. and Stepaniak, D. P.: Covariability of components of poleward atmospheric energy transports on seasonal and interannual timescales, J. Climate, 16, 3691–3705, 2003.

Wang, Y. J., Cheng, H., Edwards, R. L., An, Z. S., Wu, J. Y., Shen, C. C., and Dorale, J. A.: A High-Resolution Absolute-Dated Late Pleistocene Monsoon Record from Hulu Cave, China, Science, 294, 2345–2348, doi:10.1126/science.1064618, 2001.

Wang, P.: Seasonality over Greenland during the Holocene and possible explanations of the 8.2 kyr event – A study based on the circulation model ECBilt-CLIO, Msc Thesis, NBI, University of Copenhagen, Denmark, 2009.

Wunsch, C.: The total meridional heat flux and its oceanic and atmospheric partition, J. Climate, 18, 4374–4380, 2005.

Zhang, R. and Delworth, T. L.: Simulated tropical response to a substantial weakening of the Atlantic thermohaline circulation, J. Climate, 18, 1853–1860, 2005.

CPD
7, 1235–1259, 2011

Table 1. Experiment summary, x is the strength factor used to multiply the anomaly (x = 0.5, 1, 1.5, 2), ANO – anomaly from ECBilt-CLIO experiments.

Experiment	GHG (CO_2,N_2O,CH_4)	orbital forcing (obliq., lve, eccen.)	SST
PD_ctrl	280 ppm, 270 ppb, 760 ppb	23.446°, 102.04°, 0.016724°	Shea et al. (1992)
PD_px PD_mx	PD_ctrl	PD_ctrl	PD_ctrl + x*ANO PD_ctrl – x*ANO
LGM_ctrl	200 ppm, 190 ppb, 350 ppb	22.949°, 114.42°, 0.018994°	CLIMAP
LGM_px LGM_mx	LGM_ctrl	LGM_ctrl	LGM_ctrl + x*ANO LMG_ctrl – x*ANO

CPD
7, 1235–1259, 2011

Table 2. Resulting Northern Hemisphere meridional temperature gradients (NHTG) from the different experiments.

Experiment	NHTG (K)
PD_ctrl	20.1
PD_p0.5	19.6
PD_p1	18.9
PD_p1.5	18.4
PD_p2	17.8
PD_m0.5	20.6
PD_m1	21.4
PD_m1.5	22.1
PD_m2	22.6
LGM_ctrl	27.5
LGM_p0.5	27.1
LGM_p1	26.7
LGM_p1.5	26.5
LGM_p2	26.1
LGM_m0.5	27.85
LGM_m1	28.13
LGM_m1.5	28.5
LGM_m2	28.85

CPD
7, 1235–1259, 2011

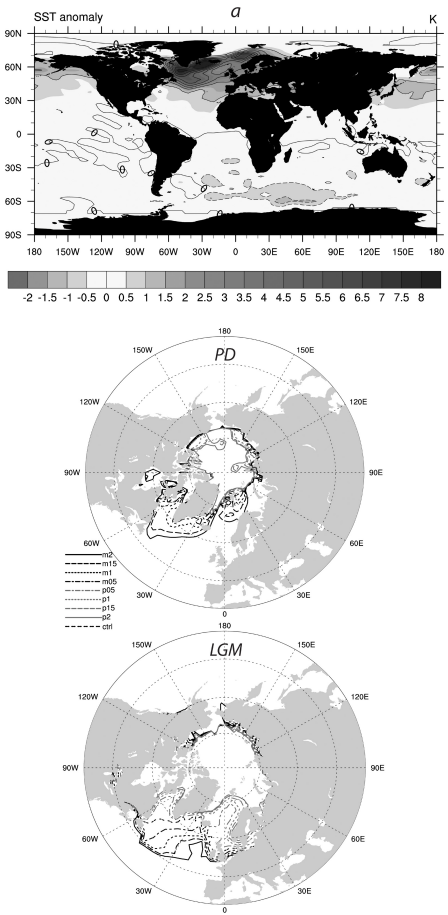

Fig. 1. (a) Annual average sea surface temperature anomalies from ECBilt-CLIO experiments. Negative anomalies: dashed (0.5 K intervals), positive anomalies: solid (1 K intervals). Panels **(b)** and **(c)** NH summer sea ice lines (−1.8 °C SST isotherms) for PD and LGM simulations, respectively.

CPD
7, 1235–1259, 2011

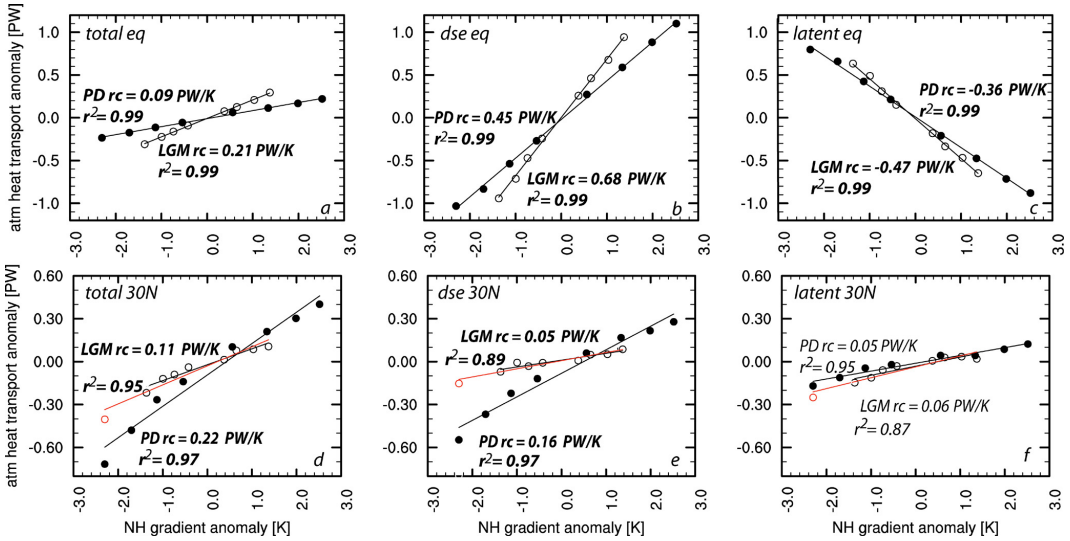

Fig. 2. Atmospheric transport anomalies (PW) at the equator **(a, b, c)** and 30° N **(d, e, f)** for PD (full circles) and LGM (open circles) simulations as a function of NHTG anomaly (K). Positive/negative NHTG anomalies refer to NH cooling/warming. Linear regression coefficients and r^2 values of the fit are indicated. Bold font indicates that the difference between PD and LGM slopes is statistically significant at the 95% level. Red open circle represents the LGM_p3 experiment.

CPD
7, 1235–1259, 2011

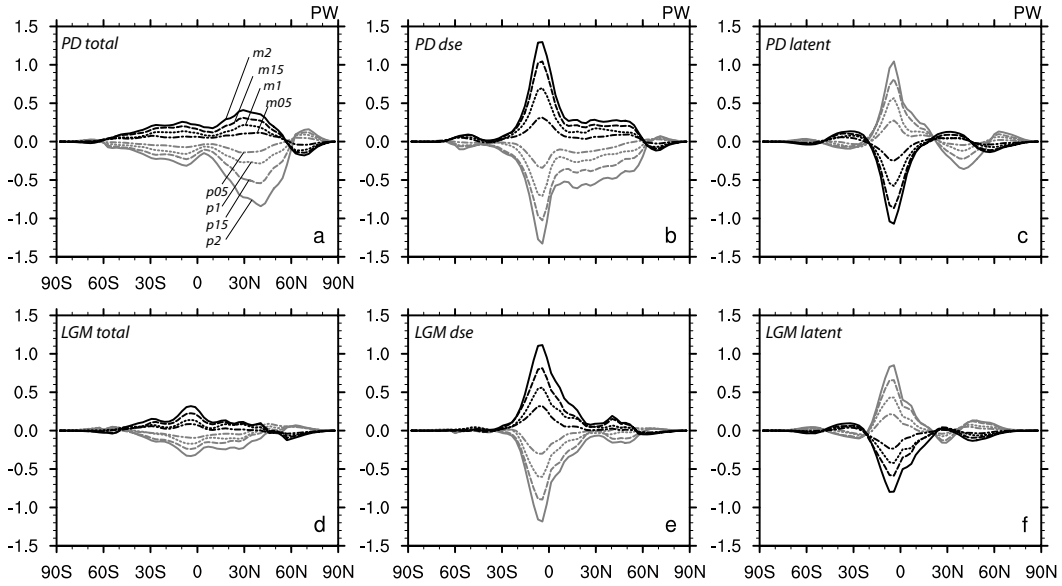

Fig. 3. Atmospheric transport anomalies: total (**a** and **d**), DSE (**b** and **e**), latent (**c** and **f**) for PD (upper plots) and LGM (lower plots) simulations. Black curves: NH cooling simulations (*m*2, *m*1.5, *m*1 and *m*0.5), grey curves: NH warming simulations (*p*2, *p*1.5, *p*1 and *p*0.5).

CPD
7, 1235–1259, 2011

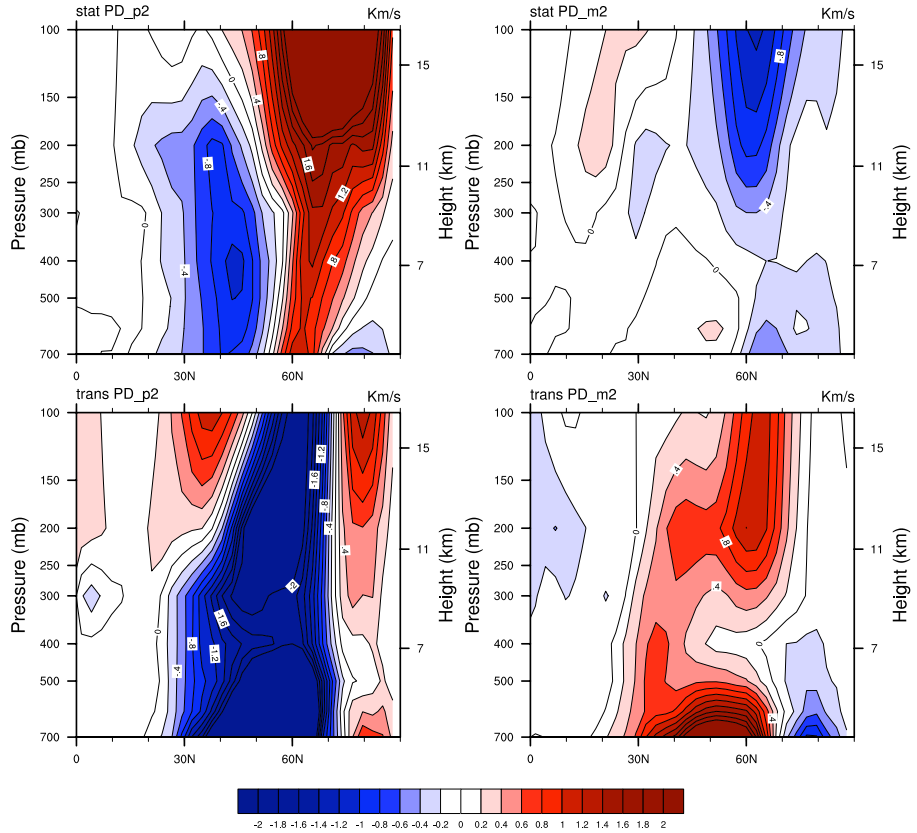

Fig. 4. Stationary (upper plots) and transient eddy (lower plots) annual heat flux anomalies for PD_m2 and PD_p2 simulations.

CPD
7, 1235–1259, 2011

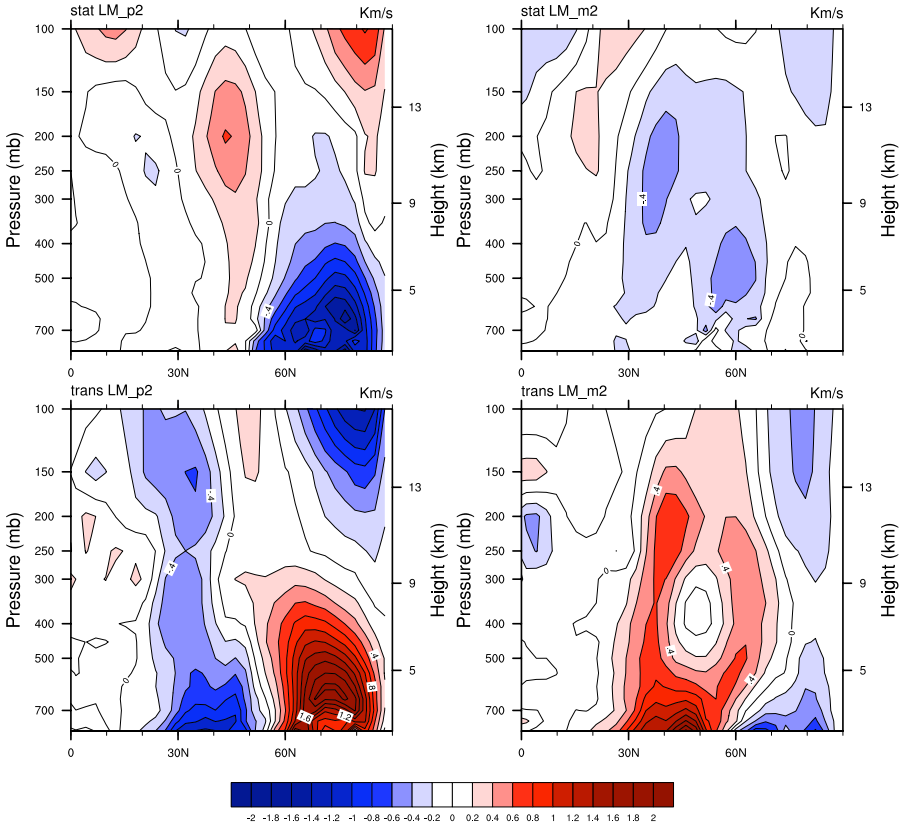

Fig. 5. Stationary (upper plots) and transient eddy (lower plots) annual heat flux anomalies for LGM_m2 and LGM_p2 simulations.

CPD
7, 1235–1259, 2011

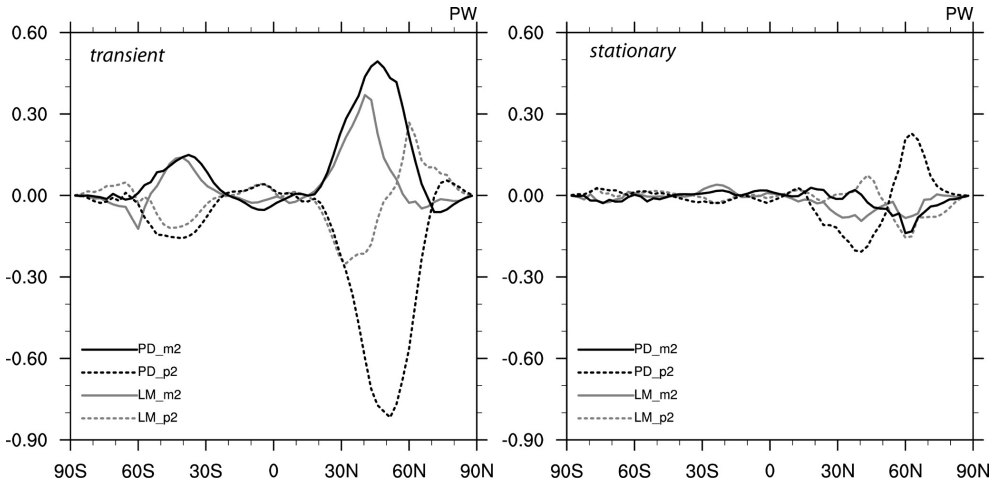

Fig. 6. Vertically integrated transient (left plot) and stationary (right plot) annual eddy heat transport anomalies for PD (black) and LGM (grey) simulations.

CPD
7, 1235–1259, 2011

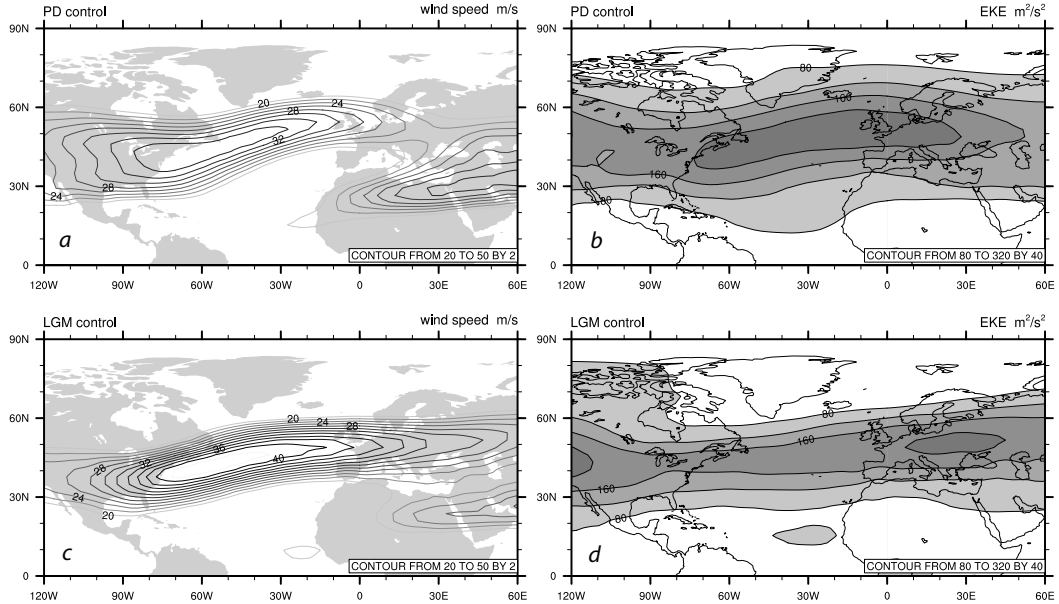

Fig. 7. Annual 200 hPa wind speeds (**a** and **c**) and eddy kinetic energies (**b** and **d**) for PD and LGM control climates.

CPD
7, 1235–1259, 2011

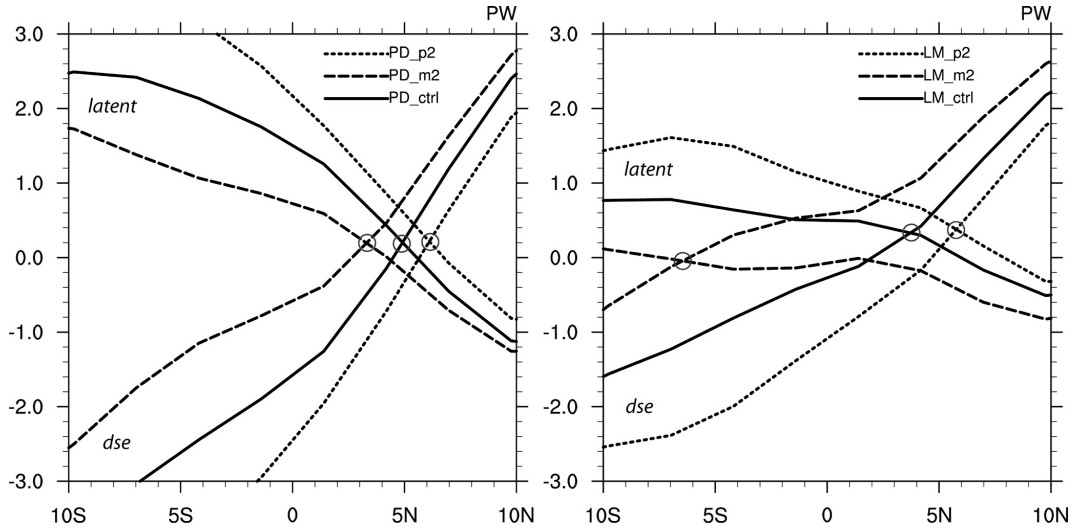

Fig. 8. Locations of annual DSE and latent heat transport crossovers in PD (left plot) and LGM (right plot) simulations.

CPD
7, 1235–1259, 2011